ACS OMEGA

http://pubs.acs.org/journal/acsodf

Article

Efficiency Maximization of a Direct Internal Reforming Solid Oxide Fuel Cell in a Two-Layer Self-Optimizing Control Structure

Shengdong Fu, Lingjian Ye,* Feifan Shen, and Yuchen He

Cite This: *ACS Omega* 2023, 8, 14558−14571

Read Online

ACCESS | Metrics & More | Article Recommendations

ABSTRACT: Control system configuration is essential for the efficiency performance of a solid oxide fuel cell (SOFC). In this paper, we aim to report a novel two-layer self-optimizing control (SOC) system for the efficiency maximization of a direct internal reforming SOFC, where the efficiency index is defined as the profit of generated electricity penalized by carbon (CO_2) emission. Based on the lumped-parameter model of the SOFC, comprehensive evaluations are carried out to identify the optimal controlled variables (CVs), the control of which at constant set-points can optimize the efficiency, in spite of operating condition changes. In the lower SOC layer, we configure single variables as the CVs. The results show that the stack temperature is the active constraint which should be controlled to maintain the cell performance. In addition, the outlet hydrogen composition is identified as the optimal CV. This result differs from several previous proposals, such as methane composition. In the presence of operating condition changes, the set-point of hydrogen composition is further automatically adjusted by the upper SOC layer, where a linear combination of the SOFC measurements is configured as the CV, giving negligible efficiency losses. The cascaded two-layer SOC structure is able to maximize the SOFC efficiency and reduce carbon emission without using online optimization techniques; meanwhile, it allows for smooth and safe operations. The validity of the new scheme is verified through both static and dynamic evaluations.

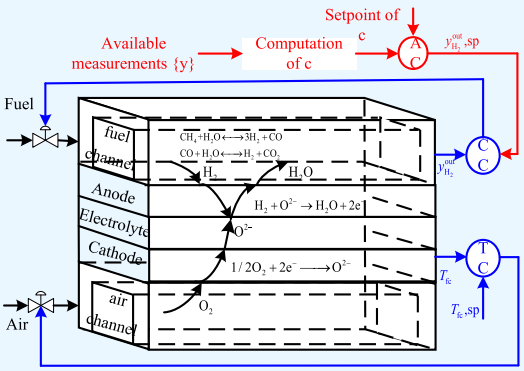

1. INTRODUCTION

The solid oxide fuel cell (SOFC) is considered as one of the most promising fuel cell technologies for cogeneration. Compared with other traditional power generation equipment, it has advantages such as no moving parts, quiet operation, low environmental pollution, high reliability, and high energy conversion efficiency.[1] Furthermore, it was found that the efficiency of a fuel cell system is almost independent of its size. Thus, smaller power plants can be developed to compete with larger centralized plants.

In fuel cell systems, hydrocarbons need to be converted into hydrogen-rich gases for electrochemical reactions.[2] One approach, known as indirect internal reforming (IIR), is to first process the fuel in an external catalytic steam reformer. However, IIR requires external heat to drive the reforming reaction, which is energy inefficient. Another method is the direct internal reforming (DIR), in which methane is fed directly into the cell and the heat inside the cell drives the reforming reaction. The trace compounds in the fuel are believed to contaminate the electrolyte or affect reforming performance. Some recent studies indicate that the influence of hydrogen sulfide can be avoided by using paper-structured catalysts or improving anode materials.[3,4] Illathukandy et al.[5] proposed that trace hydrogen chloride in biogas has little effect on the lifespan and performance of a DIR-SOFC above 1020 K.

Without an external pre-reformer, the thermal efficiency of the SOFC is further improved, and the system structure is also simpler, but the integration of reforming and the electrochemical oxidation reaction makes it challenging to operate the DIR-SOFC. DIR brings about a sudden drop in the internal temperature of the cell and greater changes in the outlet temperature.[6] In addition, the reforming reaction can also produce carbon deposition on the anode surface, damaging the cell's performance and life. Moreover, the DIR-SOFC is a complex nonlinear system, which is affected by various disturbances and uncertain parameters. In this context, the mathematical modeling and simulation, as well as advanced control system design technology, are key elements to pushing forward the success of commercialization of the DIR-SOFC.

Received: January 15, 2023
Accepted: March 27, 2023
Published: April 10, 2023

Over the past few decades, fruitful outcomes have been achieved on modeling and process simulation for the SOFC. These models range from zero-dimensional (0-D) to three-dimensional (3-D) ones, where 0-D is the lumped parameter model and the others are distributed parameter models. For cell and stack design, 2-D and 3-D ones are usually necessary[7−10] for investigating the effects of co- and counter-flows, structural and geometric configurations, etc. On the other hand, zero- and one-dimensional modeling are mostly considered for system-level control, such as predicting the transient and static responses of the fuel cell/stack under the change of operating parameters.[11] Aguiar et al.[12] concluded that the temperatures of the electrolytes, fuel and air channels, and interconnect vary significantly along the cell, but their differences at fixed points are negligible. Kang et al.[13] assumed that the cell's temperature is the same along the vertical direction and the current density distributes uniformly in the SOFC, significantly reducing the calculation time without loss of much accuracy compared with the original 1-D model. Xi et al.[14] proposed that 0-D models are accurate enough for system-level analysis through experiments. However, the zero-dimensional model ignores the distribution of internal temperature, composition, and current density and assumes that the rate of each reaction is the same everywhere in the battery, which is inconsistent with the reality. The use of a zero-dimensional model in the research of control and optimization is actually a compromise of computation.

It is known that variable analysis and control structure design are critical for operation of the SOFC. Kupecki et al.[15] analyzed the electrochemical characterization ($j-V$ curve and EIS) and outlet gas composition of the battery to observe the degradation of output performance and determine the effect of the state of the battery on the molar fraction of the outlet gas. Barelli et al.[16] used a general regression law to maintain a constant stack temperature by regulating the air flow under varying load and fuel composition. Jienkulsawad et al.[17] studied the SOFC integrated with a molten carbonate fuel cell. Different active constraints and control variables (CVs) were identified in different interference regions to ensure safe operation and economic optimization. Mojaver et al.[18] concluded that current density is the most efficient parameter for electrical power and that increased outlet temperature can significantly improve electrical and exergy efficiencies and reduce carbon dioxide emissions in the SOFC system. Kupecki et al.[6] proposed a direct internal reforming model verified by experimental data, which allows the calculation of the molar fractions of the outlet components and analyzes their impacts on the electrochemical reaction, heat balance, and mass balance. Chatrattanawet et al.[19] designed a robust model predictive control, which can control the fuel and temperature of the SOFC system at the set-point in the presence of parameter uncertainty.

The configuration of the control structure, especially the selection of CVs, is of critical importance for the operational performance of the SOFC. In the literature, the most frequently selected CVs for the SOFC are the stack temperature, cell voltage, fuel utilization, and air ratio, among many process outputs. Although tracking these variables was proved to be successful for regulatory control, their performances related to SOFC efficiency has been insufficiently assessed, which is of higher standards. In some cases, these schemes may lead to poor efficiency performances, even if their regulatory control qualities turn out to be satisfactory. In a general case, efficiency optimization calls for set-point optimization when the operating conditions change, which is however not a trivial task. In the field of process system engineering, the self-optimizing control (SOC) methodology[20] gives an alternative way to systematically evaluate the performance of candidate CVs from an optimization perspective. With suitable selections, it could be even possible to avoid the renewing of set-points if the efficiency loss is small enough. Various SOC algorithms were developed based on this idea, such as the fast identification of optimal CVs and establishing measurement combinations as the CVs. In Particular, the construction of measurement combinations as CVs was demonstrated to be promising compared with the traditional case of a single variable. A preliminary effort for SOC of the SOFC has been conducted,[1] where the stack temperature and outlet methane composition are selected as the CVs. However, this scheme turns out to be suboptimal based on our studies.

In this paper, we conduct comprehensive evaluations for configuring an SOC control system for efficiency maximization of the DIR-SOFC system, where the efficiency index is defined as the profit of generated electricity per unit weight of methane penalized by carbon tax (released CO_2 into the atmosphere). Basically, there remain two main challenges seeking such an SOC solution. The first is the identification of optimal CVs, which involves solving a large-scale optimization problem. The second is the research gap between the proposal of controlling measurement combinations and the industrial practice that favors a single physical variable as the CV, which can be better interpreted by field operators/engineers. For the first challenge mentioned above, a global SOC (gSOC) solution[21] is employed, which is able to efficiently identify self-optimizing CVs by introducing minor but reasonable approximations to the rigorous SOC formulation. A wide range of uncertain operating conditions are considered, including variations of the feed gas composition, inlet temperature, and current density. Optimal CVs are therefore selected and new insights are gained for better operation of the SOFC. Average performances under different operating conditions are evaluated and compared. For the second challenge, we configure a novel two-layer control structure, where in the lower layer the CV is the single variable while in the upper layer the CV is a measurement combination. In both layers, the CVs are self-optimizing ones to improve the SOFC efficiency. An appealing feature is that, in the proposed cascaded control layers, the set-point of the lower self-optimizing CV is automatically updated by the upper, whose set-point is constant. On one hand, the whole control structure is able to realize real-time optimization that maximizes the SOFC efficiency with negligible performance loss. On the other hand, safe operation can be conveniently guaranteed by imposing suitable lower and upper bounds for the lower CV set-point which are physical variables. The maintenance cost for the control system is saved, and the operation can be conducted monitoring whether the variables of the bottom cycle exceed the operational limits. In this way, the second challenge is circumvented.

The outcomes turn out to be interesting and promising. Compared with previous control strategies for the SOFC, their efficiency performances are thoroughly evaluated and compared. We identify that the outlet hydrogen composition $y_{H_2}^{out}$ is the best single-variable CV. Interestingly, this is similar

https://doi.org/10.1021/acsomega.3c00293
ACS Omega 2023, 8, 14558−14571

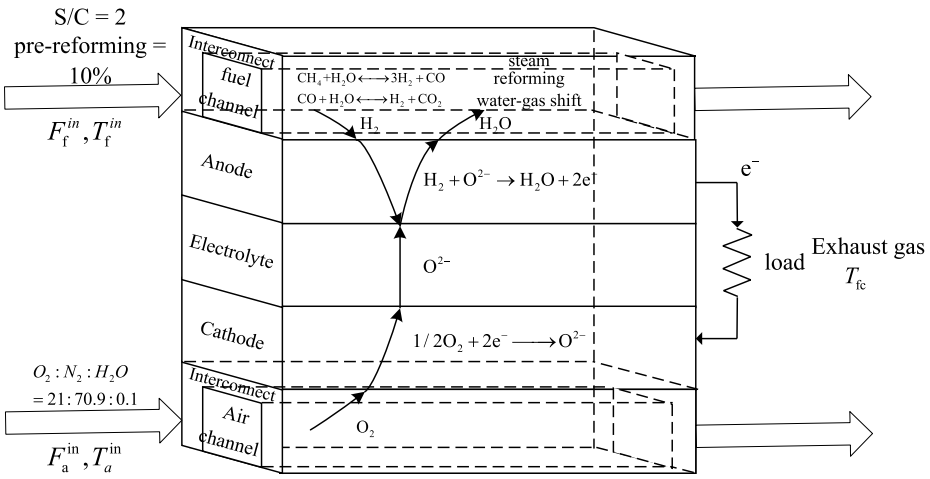

Figure 1. Schematic diagram of SOFC unit.

to controlling the popular fuel utilization in many existing works. Similarities and differences are thus discussed and compared. More importantly, the set-point of $y_{H_2}^{out}$ in this study can be further optimized via tracking the constant set-point of the upper layer CV,which is a measurement combination constituted by $y_{H_2}^{out}$, $y_{CO_2}^{out}$ (outlet CO_2 composition), and V_{fc} (output voltage).

Such a strategy shares many advantages and has not been reported for optimization of the SOFC, to the best knowledge of the authors.

2. SOFC PROCESS

2.1. Process Descriptions. The complete SOFC stack consists of several identical electrochemical cells connected in series or parallel. It is often sufficient to study the smallest cell module located at the center of the stack. In general, the end effects for boundary cells are ignored due to their negligible influences.

The minimum unit of a planar DIR-SOFC is shown in Figure 1, which comprises the fuel and air channels, the positive-electrode/electrolyte/negative-electrode (PEN) structure, and the interconnect. Natural gas and water vapor is fed into the fuel channel, where methane is converted to hydrogen, carbon monoxide, and carbon dioxide; no occurrence of electrochemical oxidization is assumed.[12] Thus, the fuel channel consists of components such as CH_4, H_2O, CO, H_2, and CO_2, while the air channel contains O_2 and N_2.

The mechanism of chemical reactions for electricity generation is shown in Table 1. First, hydrocarbon gas in the fuel channel is converted to hydrogen by steam reforming and water gas shift (WGS) reactions. Oxygen is reduced to oxygen ions at the cathode, passing through the ion-conducting electrolyte to the anode/electrolyte interface and reacting with hydrogen to form water, waste, and electrons. Electrons return to the cathode/electrolyte interface through the external circuit.

Table 1. Reactions in an SOFC

reaction name	reaction equation	ΔH (kJ/mol)
steam reforming	(i) $CH_4 + H_2O \leftrightarrow 3H_2 + CO$	206.10
water gas shift	(ii) $CO + H_2O \leftrightarrow H_2 + CO_2$	−41.15
hydrogen oxidation	(iii) $H_2 + O^{2-} \rightarrow H_2O + 2e^-$	–
oxygen reduction	(iv) $1/2O_2 + 2e^- \rightarrow O^{2-}$	–
overall cell	(v) $H_2 + 1/2O_2 \rightarrow H_2O$	−241.83

The following assumptions are made for the model development:

(i) The temperature and pressure inside the battery are equal everywhere.

(ii) Heat loss due to ambient temperature is ignored.

(iii) All gases are ideal.

(iv) Ignore the pressure variation along the gas passage.

The development of the lumped parameter (0-D) model here is based on the fact that a 0-D model can well capture the steady-state and transient responses of key variables[1,14,22,23] and thus is sufficient for our purpose. Note that, due to the difficulties of measuring internal distributions in practice, 2-D and 3-D models cannot be generally used for control and optimization of the SOFC.[24,25]

2.2. Mechanistic Model. The lumped parameter model of the SOFC is established based on mass balance, energy balance, and electrochemical models. The mass balance in the fuel and air channels is expressed as the change of the gas composition; that is, after consideration of the reaction rate of the components, the molar rate of the outlet gas minus the molar rate of the inlet gas is equal to the concentration change of the internal gas components of the cell.

fuel channel:

$$\frac{dn_{i,f}}{dt} = F_{i,f}^{in} - F_{i.f}^{out} + \sum_{k\in\{(i),(ii),(v)\}} v_{i,k}R_kA \quad (1)$$

where i = CH_4, H_2O, CO, H_2, and CO_2.

air channel:

$$\frac{dn_{i,a}}{dt} = F_{i,a}^{in} - F_{i,a}^{out} + v_{i,(v)}R_{(v)}A \quad (2)$$

where i = $_2$ and N_2.

For the energy balance, the dynamic equation of the fuel cell temperature can be expressed as eq 3, under the assumption that the temperature variation inside the cell is negligible.

https://doi.org/10.1021/acsomega.3c00293
ACS Omega 2023, 8, 14558−14571

Table 2. Specific Heat Capacity Constant of Each Component

component	A	B	C	D	E
steam	33.93	-8.42×10^{-3}	2.99×10^{-5}	-1.78×10^{-8}	3.69×10^{-12}
carbon monoxide	29.56	-6.58×10^{-3}	2.01×10^{-5}	-1.22×10^{-8}	2.26×10^{-12}
carbon dioxide	27.44	4.23×10^{-2}	-1.96×10^{-5}	4.00×10^{-9}	-2.99×10^{-13}
hydrogen	25.40	2.02×10^{-2}	-3.86×10^{-5}	3.19×10^{-8}	-8.76×10^{-12}

$$\frac{dT_{fc}}{dt} = \frac{1}{\rho_{SOFC} C p_{SOFC} V_{SOFC}} (\dot{Q}_{f,in} - \dot{Q}_{f.out} + \dot{Q}_{a,in} - \dot{Q}_{a,out} + \sum_{k\in\{(i),(ii),(v)\}} (-\Delta H)_k R_k A - jAV_{fc}) \quad (3)$$

where

$$\dot{Q}_j = \sum_i F_i C p_i (T_j - T_{ref}) \quad (4)$$

The right-hand-side terms in eq 3 represent the total input heat, total output heat, heat absorption and release, and electric energy output, respectively. The specific heat capacity of each component gas can generally be calculated by the following formula:

$$C_p = A + BT + CT^2 + DT^3 + ET^4 \quad (5)$$

The values of specific heat capacity constants A, B, C, and D of each gas are given in Table 2.[26]

Different kinetics for chemical reactions were reported in the literature,[27] depending on various factors such as the anode material, temperature, and steam to carbon ratio. The following kinetics[1] are considered in this study, which have been widely used for SOFC studies. In eq 7, h_f is the height of the fuel channel.

$$R_{(i)} = k_0 p_{CH_4} \exp\left(-\frac{E_a}{RT_{fc}}\right) \quad (6)$$

$$R_{(ii)} = k_{WGSR} p_{CO} p_{H_2O} h_f \left(1 - \frac{p_{CO_2} p_{H_2O} / p_{CO} p_{H_2O}}{K_{eq}}\right) \quad (7)$$

$$K_{eq} = \exp\left(\frac{4276}{T_{fc}} - 3.961\right) \quad (8)$$

$$k_{WGSR} = 0.0171 \exp\left(\frac{-103191}{RT_{fc}}\right) \quad (9)$$

$$R_{(v)} = \frac{j}{2F} \quad (10)$$

The electrochemical models are as follows. The operating voltage, V_{fc}, is calculated as the difference between the open-circuit voltage and the overpotential loss, as well as the ohmic loss.

operating voltage:

$$V_{fc} = E_{OCV} - (\eta_{ohm} + \eta_{conc,anode} + \eta_{conc,cathode} + \eta_{act,anode} + \eta_{act,cathode}) \quad (11)$$

The theoretical open-circuit voltage depends on the electrode's local gas composition and temperature and can be determined by the Nernst equation (eq 12) of hydrogen.

$$E_{OCV} = E_0 - \frac{RT_{fc}}{2F} \ln\left(\frac{p_{H_2O}}{p_{H_2} p_{O_2}^{1/2}}\right) \quad (12)$$

where E_0 represents the open-circuit voltage at standard pressure and operating temperature, given by

$$E_0 = 1.253 - (2.4516 \times 10^{-4}) T_{fc} \quad (13)$$

Ohmic losses are mainly due to resistance to ion conduction in the electrolyte, resistance to electron conduction in the electrode and current collector, and, to a lesser extent, contact resistance between cell components. Ohmic losses can be expressed by

$$\eta_{ohm} = jAR_{ohm} = jA\left(\frac{\tau_{anode}}{\sigma_{anode}} + \frac{\tau_{electrolyte}}{\sigma_{electrolyte}} + \frac{\tau_{cathode}}{\sigma_{cathode}}\right) \quad (14)$$

A local drop in potential occurs when fuel reaction rate is too fast, resulting in a scarcity of reactants. This corresponding loss of output voltage, known as concentration overpotential, can be expressed as follows.

$$\eta_{conc} = \frac{RT_{fc}}{2F} \ln\left(\frac{p_{H_2O,TPB} p_{H_2,f}}{p_{H_2O,a} p_{H_2,TPB}}\right) + \frac{RT_{fc}}{4F} \ln\left(\frac{p_{O_2,a}}{p_{O_2,TPB}}\right) \quad (15)$$

The partial pressure at the three-phase boundary (TPB) needs to be calculated to derive the concentration overpotential.

$$p_{H_2,TPB} = p_{H_2,f} - \frac{RT_{fc}\tau_{anode}}{2F\overline{D}_{eff,anode}} j \quad (16)$$

$$p_{H_2O,TPB} = p_{H_2O,f} + \frac{RT_{fc}\tau_{anode}}{2F\overline{D}_{eff,anode}} j \quad (17)$$

$$p_{O_2,TPB} = P - (P - p_{O_2,a}) \exp\left(\frac{RT_{fc}\tau_{cathode}}{4FD_{eff,cathode}P} j\right) \quad (18)$$

The activation overpotential reflects the kinetics of the electrode/electrolyte interface. The following equation is a Butler–Volmer nonlinear equation that relates the local current density to the activation overpotential.

$$j = j_{0,anode}\left[\frac{p_{H_2,TPB}}{p_{H_2,f}} \exp\left(\frac{\alpha nF}{RT_{fc}}\eta_{act,anode}\right) - \frac{p_{H_2O,TPB}}{p_{H_2O,f}} \exp\left(-\frac{(1-\alpha)nF}{RT_{fc}}\eta_{act,anode}\right)\right] \quad (19)$$

https://doi.org/10.1021/acsomega.3c00293
ACS Omega 2023, 8, 14558−14571

$$j = j_{0,\text{cathode}}\left[\exp\left(\frac{\alpha nF}{RT_{\text{fc}}}\eta_{\text{act,cathode}}\right) - \exp\left(-\frac{(1-\alpha)nF}{RT_{\text{fc}}}\eta_{\text{act,cathode}}\right)\right] \quad (20)$$

where

$$j_{0,\text{electrode}} = \frac{RT_{\text{fc}}}{nF}k_{\text{electrode}}\exp\left(-\frac{E_{\text{electrode}}}{RT_{\text{fc}}}\right)$$

$$\text{electrode} \in \{\text{anode, cathode}\} \quad (21)$$

Equations 1−20 are the governing equations for describing the SOFC being studied. It is also stressed that these equations are coupled and should be solved as equality constraints due to their couplings.

2.3. Model Validation. In this paper, the lumped parameter model is simulated on Matlab. The electrochemical model allows calculation of the output voltage, current density, and power density of the SOFC. Figure 2 compares the predicted SOFC operating voltage of the model with the existing experimental data. In Zhao and Virkar's research,[28] a mixture of 10% H_2 and 90% N_2 was circulated on the anode side and air was injected into the cathode. The flow rates of hydrogen and air were 300 and 550 mL·min^{-1}, respectively. Voltage versus current density polarization curves were obtained over a range of temperatures between 873 and 1073 K. The comparison of simulation and experimental data under the same conditions verifies the accuracy of the model.

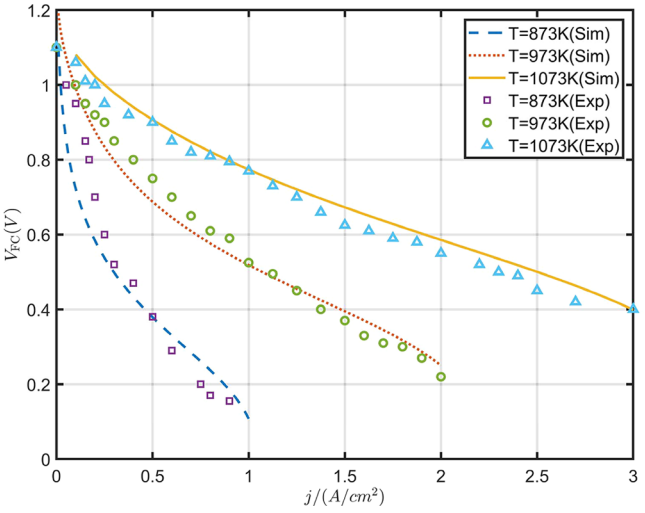

Figure 2. Model prediction accuracy.

2.4. Operational Objective. For the safe and smooth operation of the SOFC, the following process constraints should be respected.[2]

- The feed temperature of the fuel channel is between 993 and 1053 K.
- The feed temperature of the air channel is between 993 and 1053 K.
- The maximum total temperature difference ($T_{\text{fc}} - T_{\text{in}}$) along a 40 cm cell is 400 K.
- The minimum cell voltage is 0.55 V. Lower battery voltage can lead to anodic oxidation.
- The fuel efficiency (U_{f}) is maintained below 85%. Excessive fuel efficiency will result in nickel oxide formation and reduced electrolyte activity.
- The system's allowable air ratio (λ_{air}) is between 2 and 14, which meets the minimum stoichiometry requirements and is within the compressor's maximum allowable air flow rate.
- With the increase of the internal temperature, the cell efficiency and power first increase and then decrease.[12,29] Therefore, an upper limit is often set for the outlet temperature of the cell to maintain the stability of the output performance.

One main task for the SOFC is to follow the power demand required by the load, which is often satisfied by changing the current density drawn from the SOFC. In this case, there are two degrees of freedom (manipulated variables, MVs) for operation, namely, the inlet molar rates of the fuel, F_{f}^{in}, and air, F_{a}^{in}. These two MVs should be operated to satisfy various process requirements.

In this paper, we aim to maximize the cell's efficiency, which is defined as the profit of power generation per unit weight of methane excluding the cost of methane. In addition, we consider the detrimental effect of CO_2 released to the atmosphere. A penalty term representing the carbon tax is added within the efficiency expression, which encourages cleaner production along with the maximization of the overall efficiency.

$$\zeta = \frac{P_{\text{w}}P_{\text{ele}}}{\dot{m}_{\text{CH}_4}^{\text{in}}} - \frac{\dot{m}_{\text{CO}_2}\text{Tax}_{\text{CO}_2}}{\dot{m}_{\text{CH}_4}^{\text{in}}} - P_{\text{CH}_4}\ [(\text{CNY·t of CH}_4)^{-1}] \quad (22)$$

An important characteristic considered in this paper is that the efficiency will be maximized under changing operating conditions. Experiences show that these uncertainties can be attributed to parametric changes of the fuel components, inlet temperatures in the two channels, the inner temperature constraint, and the average current density, as summarized in Table 3. The nominal parameters are determined from industrial data.[12] The system feeds a mixture of methane and water to the SOFC. Assuming that the raw material has undergone 10% pre-reforming, the inlet fuel is a gas mixture of CH_4, CO, H_2O, H_2, and CO_2.

Table 3. Disturbances to Select Economic CVs

symbol	representation	nominal value	expected variation
d_1	current density	0.5 A/cm^2	±50%
d_2	steam to carbon ratio	2	±25%
d_3	pre-reforming	10%	±25%
d_4	inlet temperature of fuel/air	1023 K	±30 K

In the nominal case, the inlet molar flow rates of fuel and air can be numerically obtained by maximizing eq 22, and the optimal solutions are 0.0010 and 0.206 mol/s. Unfortunately, the established operational strategy is unrealistic because it is open loop and will lead to infeasibility where the constraints are violated due to the varying operating conditions. Figure 3 shows an overview of the optimal feed rates performing parametric optimization problems for independent realizations of the disturbances defined above, where it is evident that the desired optimal operation is susceptible to disturbances. Meanwhile, it is unrealistic to perform such repeated optimizations in a practice case, because the uncertain disturbances could be unknown in general.

https://doi.org/10.1021/acsomega.3c00293
ACS Omega 2023, 8, 14558−14571

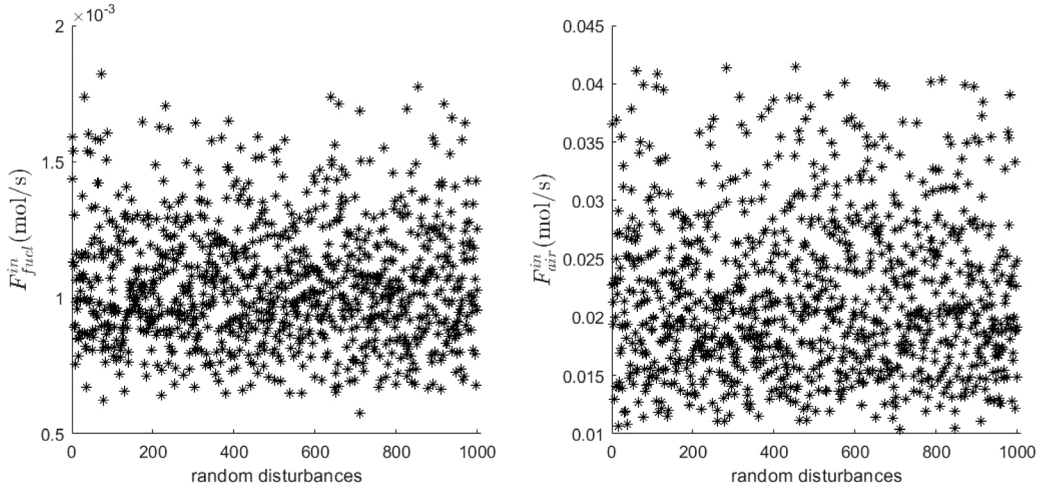

Figure 3. Optimal feed rates under random disturbances.

With the increase of temperature, the power and efficiency of the battery tend to increase first and then decrease. In the process design, in order to stabilize the output performance, we generally impose an upper bound on the outlet temperature of the battery. In addition to the consideration of efficiency, limiting the outlet temperature is also conducive to the control of the local temperature gradient. Chatrattanawet[1] believes that there is an active constraint on the SOFC temperature and maintains the temperature at 1069 K. However, Jienkulsawad[17] proposed that the temperature difference between the outlet and the inlet is less than or equal to 400 K, which can meet the safety requirements of the process. The upper bound of the outlet temperature should be set more to maximize the power demand and economic benefits. Therefore, the upper bound of the temperature is set to 1100 K later, which increases the cell efficiency compared with 1069 K while meeting the safety constraints. According to the static calculation, the temperature constraint, $T_{fc} \leq 1100$ K, is always active at the upper bound. This result coincides with the situation in which T_{fc} is a typical CV in many open studies.[16,17,30−33]

3. SELF-OPTIMIZING CONTROL

3.1. Methodology Description. Control of the stack temperature, T_{fc}, consumes one degree of freedom, which leaves with one additional CV to be determined. In this paper, selection of the remaining CV is carried out by full evaluation of the cell's closed-loop efficiency when the operating conditions vary. Such an idea was termed as the SOC for control structure design of chemical processes.[20]

Let the operational optimization problem be formulated as

$$\begin{aligned} &\min_{u} J(u, d) \\ &\text{s.t.} \quad G(u, d) \leq 0 \end{aligned} \tag{23}$$

where J is a general cost function to be minimized (which, in this study, is $J := -\zeta$, the negative SOFC efficiency); $u \in R^{n_u}$ and $d \in R^{n_d}$ are controlled variables and uncertain disturbances/parameters, respectively; G are process constraints.

The criterion considered by SOC is given as solving the following optimization problem:

$$\begin{aligned} &\min_{c \in \{y\}} \int_{d \in \mathcal{D}} \int_{n \in \mathcal{N}} J(u, d)\, \mathrm{d}n\, \mathrm{d}d \\ &\text{s.t.} \quad G(u, d) \leq 0 \\ &y_m = y + n = f(u, d) + n \\ &c = c_s \end{aligned} \tag{24}$$

where y, n, and y_m are process output variables and their noise and true measurements; c and c_s are the controlled variables and set-points; f is the output model.

One notes that SOC aims to minimize the cost function by selecting c in the set $\{y\}$, while conventional methods usually focus on the controllability and control performance. Furthermore, lower control loops can be configured in the SOC for the regulatory control purpose; thus they are not contradictory. In general, the SOC method combines optimization with feedback regulation to improve the convergence to the optimal speed, which distinguishes from the common real-time optimization schemes.

Assuming that the constraints G can be either actively controlled or maintained in the feasible range (for the SOFC, the cell temperature is an active constraint), the efficiency performances of existing control strategies for the SOFC can be systematically evaluated, by calculating the objective function in (24). For example, in the case where the output voltage is controlled at 0.7 V, the average efficiency index is computed as

$$\begin{aligned} &\bar{\zeta} = \int_{d \in \mathcal{D}} \int_{n_{V_{fc}} \in \mathcal{N}} \zeta\, \mathrm{d}n_{V_{fc}}\, \mathrm{d}d \\ &\text{s.t.} \quad \text{SOFC model} \\ &V_{fc} + n_{V_{fc}} = 0.7 \text{ V} \end{aligned} \tag{25}$$

where the domains $\mathcal{D}$ and $\mathcal{N}$ can be discretized to compute the integrand for $\bar{\zeta}$. Similar computations are followed by replacing the last constraint for other control schemes. These computations and comparisons are presented in section 4.1.

In general, however, one is required to solve the full optimization problem (24) to identify the optimal CV among the full measurement set, which is a combinational optimization problem and is computationally prohibitive, in the case of an exhaustive search when the number of candidate CVs is large. Several fast screening algorithms have been

https://doi.org/10.1021/acsomega.3c00293
ACS Omega 2023, 8, 14558−14571

developed to deal with this difficulty, e.g., the branch and bound algorithm based on the maximum gain rule,[34−37] which linearizes the process model and introduces big approximations.

3.2. Measurement Combination as the CV. Theoretical analysis shows that the SOC performance can be greatly enhanced by controlling some functional of measurements (artificial variables). The most popular and obvious such artificial variables are the linear combinations of measurements, denoted by $c = Hy$. In this case, (24) is extended to the form of

$$\begin{aligned} &\min_{H} \int_{d\in\mathcal{D}} \int_{n\in\mathcal{N}} J(u, d)\, \mathrm{d}n\, \mathrm{d}d \\ &\text{s.t.} \quad G(u, d) \le 0 \\ &y_{\mathrm{m}} = y + n = f(u, d) + n \\ &Hy = c_{\mathrm{s}} \end{aligned} \tag{26}$$

which is even more complicated compared with (24), as the decision space of H could be infinite.

A number of approaches were developed to solve (26), mostly with substantial simplifications to derive a tractable formulation. In particular, most methods employed linearization of the process model, f, around the nominal point,[38−41] which leads to a large error when interference causes equipment to deviate from the nominal point. On the contrary, the recently established global SOC (gSOC) approach[21] is able to eliminate the error caused by linearization and turned out to be promising with an efficient solution approach. A sketch of the gSOC method is outlined as follows.

Consider the second-order Taylor expansion for J in terms of c at the optimal point:

$$J = J^{\mathrm{opt}} + J_c^{\mathrm{T}} e_c + 0.5 e_c^{\mathrm{T}} J_{cc} e_c \tag{27}$$

where J_c and J_{cc} are the Jacobian and Hessian matrices, respectively; $e_c = c - c^{\mathrm{opt}}$ is the deviation of c from the optimum. According to the optimality condition and the definition of c, it follows that $J_c = 0$ and $e_c = -Hy_{\mathrm{m}}^{\mathrm{opt}}$, where $y_{\mathrm{m}}^{\mathrm{opt}} = y^{\mathrm{opt}} + n$ is the optimal measurement corrupted by noise. Therefore, the loss L is expressed as a quadratic function:

$$L = J - J^{\mathrm{opt}} = 0.5 e_c^{\mathrm{T}} J_{cc} e_c = 0.5 (Hy_{\mathrm{m}}^{\mathrm{opt}})^{\mathrm{T}} J_{cc} (Hy_{\mathrm{m}}^{\mathrm{opt}}) \tag{28}$$

Over discretized operating conditions, the average loss $L_{\mathrm{av}} = E[L]$, is approximated as

$$L_{\mathrm{av}} \approx \frac{1}{2N} \sum_{i=1}^{N} (Hy_{(i)}^{\mathrm{opt}})^{\mathrm{T}} J_{cc} Hy_{(i)}^{\mathrm{opt}} + \frac{1}{2} \mathrm{tr}(W_n^{\,2} H^{\mathrm{T}} J_{cc} H) \tag{29}$$

where tr( ) is the trace of a matrix, N is the number of total operating conditions, and $W_n^{\,2} = E(nn^{\mathrm{T}})$ is the covariance matrix for measuring noise.

By introducing a constraint of $HG_y = J_{uu}^{\,1/2}$[21] (without loss of generality), where G_y is the input-output gain matrix at a reference point, J_{uu} is the Hessian matrix of J respect to u. In this case, $J_{cc} := J_{uu}^{\,1/2} (HG_y)^{-1} = I$, the loss function can be simplified as

$$L_{\mathrm{av}} = \frac{1}{2N} \left\| YH^{\mathrm{T}} \right\|_F^{\,2} + \frac{1}{2} \left\| W_n H^{\mathrm{T}} \right\|_F^{\,2} = \frac{1}{2} \left\| \tilde{Y} H^{\mathrm{T}} \right\|_F^{\,2} \tag{30}$$

where

$$Y = \begin{bmatrix} (y_{(1)}^{\mathrm{opt}})^{\mathrm{T}} \\ \vdots \\ (y_{(N)}^{\mathrm{opt}})^{\mathrm{T}} \end{bmatrix}, \qquad \tilde{Y} = \begin{bmatrix} \frac{1}{\sqrt{N}} Y \\ W_n \end{bmatrix} \tag{31}$$

The final optimization problem is obtained as

$$\begin{aligned} &\min_{H} L_{\mathrm{av}} = \min_{H} \frac{1}{2} \left\| \tilde{Y} H^{\mathrm{T}} \right\|_F^{\,2} \\ &\text{s.t.} \quad HG_y = J_{uu}^{\,1/2} \end{aligned} \tag{32}$$

The derivation of the solution to the above optimization problem is somewhat theoretically involved; readers can refer to ref 21 for detailed theoretical developments. Overall, it was shown that an analytic expression for H can be obtained as follows:

$$H^{\mathrm{T}} = (\tilde{Y}^{\mathrm{T}} \tilde{Y})^{-1} G_{y,\mathrm{ref}} (G_{y,\mathrm{ref}}^{\mathrm{T}} (\tilde{Y}^{\mathrm{T}} \tilde{Y})^{-1} G_{y,\mathrm{ref}})^{-1} J_{uu,\mathrm{ref}}^{\,1/2} \tag{33}$$

To sum up, the steps of the global self-optimization control method are as follows:

Step 1. Discretize the disturbance domain $\mathcal{D}$ using Monte Carlo sampling; a sequence of disturbance scenarios $\{d_{(i)}\}$, $i = 1, ..., N$ is generated.

Step 2. Perform offline optimization problem (23) for each $d_{(i)}$, and the measurements $y_{(i)}^{\mathrm{opt}}$ corresponding to the optimal solution are obtained.

Step 3. Select a reference point (e.g., the nominal point), and evaluate the Hessian of cost function $J_{uu,\mathrm{ref}}$ and the measurement sensitivity matrices $G_{y,\mathrm{ref}}$.

Step 4. Construct the intermediate matrices Y and $\tilde{Y}$.

$$Y = [y_{(1)}^{\mathrm{opt}} \quad \cdots \quad y_{(N)}^{\mathrm{opt}}]^{\mathrm{T}}, \qquad \tilde{Y} = \left[\frac{1}{\sqrt{N}} Y^{\mathrm{T}} \quad W_n \right]^{\mathrm{T}} \tag{34}$$

Step 5. The optimal combination matrix H is solved as

$$H^{\mathrm{T}} = (\tilde{Y}^{\mathrm{T}} \tilde{Y})^{-1} G_{y,\mathrm{ref}} (G_{y,\mathrm{ref}}^{\mathrm{T}} (\tilde{Y}^{\mathrm{T}} \tilde{Y})^{-1} G_{y,\mathrm{ref}})^{-1} J_{uu,\mathrm{ref}}^{\,1/2} \tag{35}$$

The above steps of the gSOC algorithm can be applied to solve the optimal combination matrix for a given set of measurements. Different subsets of measurements need to be calculated and compared to select the right combination from considerable measurements. In some problems, the number of subsets is very substantial, so the pruning method mentioned in ref 35 can be used to reduce the selection difficulty. It is also worth mentioning that when the set y is appended with an artificial measurement, $y_0 = 1$, the coefficients in H associated with y_0 are the negative optimal set-points, which is advantageous over most other approaches where c_{s} is simply taken as the nominal value of c.

3.3. Two-Layer Design Method. The measurement combination, $c = Hy$, is expected to enhance the performance by manipulating u to maintain c at constant set-points. However, as we have communicated with the industry community, an underlying inconvenience is that c may lack physical interpretations that can be understood by field operators/engineers. Furthermore, the SOC scheme may also fail when the true characterizations of the SOFC process cannot be well described by the parametric model in section 2. In this case, it will be detrimental to the plant operation.

In this paper, a two-layer SOC structure will be designed for the SOFC, such that the efficiency and practical implementa-

https://doi.org/10.1021/acsomega.3c00293
ACS Omega 2023, 8, 14558−14571

tions are both taken care of. It is a cascaded control structure: in both layers the CVs are selected based on the SOC criterion maximizing the efficiency. The lower loop is configured with a single physical variable as the CV, while the upper loop is a measurement combination to improve the efficiency, by adjusting the set-point of the lower variable. For both the lower and upper CVs, the same gSOC algorithm in section 3.2 is applied, by feeding the algorithm with different measurement sets $\{y\}$. It is easy to understand that, provided with the same topmost CVs, the static performances of a two-layer control structure and a single-layer one are equivalent. However, the benefit of the former is that the real-time set-point of lower loops, which are physical variables, can be displayed and constrained within safe bounds. This interface is particularly useful for online control and monitoring for the SOFC. Furthermore, more insights are gained along designing such a control structure as illustrated in section 4.

Remark. The classical two-layer architecture has been long prevalent and quite standard in the chemical industry, in which performing control and optimization independently are standard.[42] A new feature of the proposed two-layer SOC is that both layers serve to maximize the SOFC efficiency but are implemented via the feedback control means. This means that the task of adjusting set-points does not require disturbance estimation or reoptimization but does require computationally cheap feedback controllers. Since the SOFC stack is a relatively small-scale utility, the final obtained SOC solution can be easily programmed on portable microchips instead of needing a powerful computer to solve expansive online optimization problems.

4. RESULTS AND DISCUSSION

4.1. Evaluation of Classical Control Strategies. In past research, cell temperature was often considered as a common CV regulated by the inlet air flow. The cell temperature directly affected the reaction process and the cell life. Meanwhile, researchers also selected other physical variables as CVs, such as fuel utilization, air ratio, and outlet gas component. The choice of these variables was mostly based on the controllability analysis rather than system efficiency. Motivated by this consideration, we evaluate their efficiency performances as proposed in (25).

Table 4 shows the losses of the efficiency index of the SOFC system when CVs are controlled in the classical control strategies.

Table 4. Average and Worst Losses with a Single Measurement as the Controlled Variable

univariate measurement	reference	average loss (CNY·t^{-1})	worst loss (CNY·t^{-1})
$y^{out}_{H_2}$	Jienkulsawad et al.,[17] Taghizadeh et al.[43]	31.77	122.08
V_{fc}	Hajimolana and Soroush,[32] Sendjaja and Kariwala,[44] de Avila Ferreira et al.[45]	89.99	246.37
U_f	Jienkulsawad et al.,[17] Sendjaja and Kariwala,[44] Arpino et al.[46]	104.86	395.09
λ_{air}	Aguiar et al.,[12] Zhang et al.[30]	253.25	1179.82
P_w	Larosa et al.,[47] Huang et al.[48]	595.17	1648.90
$y^{out}_{CH_4}$	Chatrattanawet et al.[1]	625.98	1597.28

Table 5. Promising Measurement Subsets for CV Selection

n_y	promising subset	average loss (CNY·t^{-1})	worst loss (CNY·t^{-1})
1	$y^{out}_{H_2}$	31.77	112.70
2	$y^{out}_{H_2}$, V_{fc}	2.49	19.39
3	$y^{out}_{H_2}$, $y^{out}_{CO_2}$, V_{fc}	0.59	4.99
4	$y^{out}_{H_2}$, $y^{out}_{CO_2}$, V_{fc}, U_f	0.51	4.42
5	$y^{out}_{H_2}$, $y^{out}_{CO_2}$, F^{out}_f, V_{fc}, U_f	0.48	3.75
6	$y^{out}_{CH_4}$, $y^{out}_{H_2}$, $y^{out}_{CO_2}$, F^{out}_f, V_{fc}, U_f	0.43	3.46
7	$y^{out}_{CH_4}$, $y^{out}_{H_2}$, $y^{out}_{CO_2}$, F^{out}_f, V_{fc}, U_f, F^{in}_f	0.43	3.44

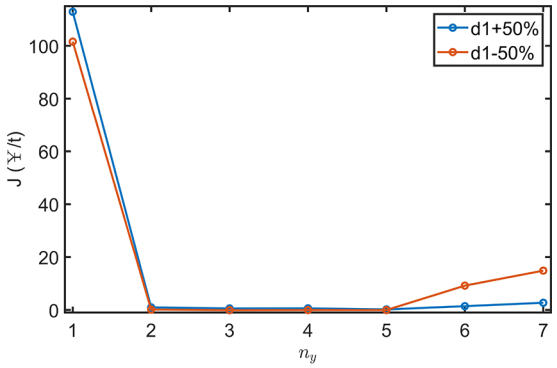

(a) Loss due to current density

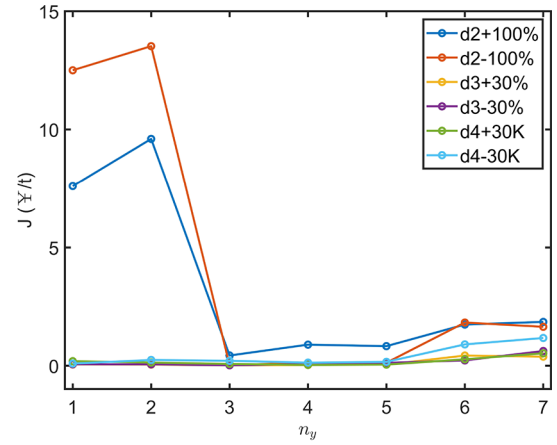

(b) Loss due to other interference

Figure 4. Economic loss caused by interference under different CV schemes.

Table 6. Parameters of the PI Controllers

loop	MV	CV	proportional gain	integral time
1	F^{in}_f	$y^{out}_{H_2}$	0.001	5
2	F^{in}_a	T_{fc}	−0.0001	20
3	c	$y^{out}_{H_2,sp}$	0.001	10

It is clearly shown that $y^{out}_{H_2}$ is an excellent choice in terms of decreasing efficiency loss, which directly represents the actual fuel consumption within the cell and is closely related to the current density. The effect after hydrogen is voltage and fuel utilization. It is understandable that the effect of power control is not good because the current density varies greatly.

https://doi.org/10.1021/acsomega.3c00293
ACS Omega 2023, 8, 14558−14571

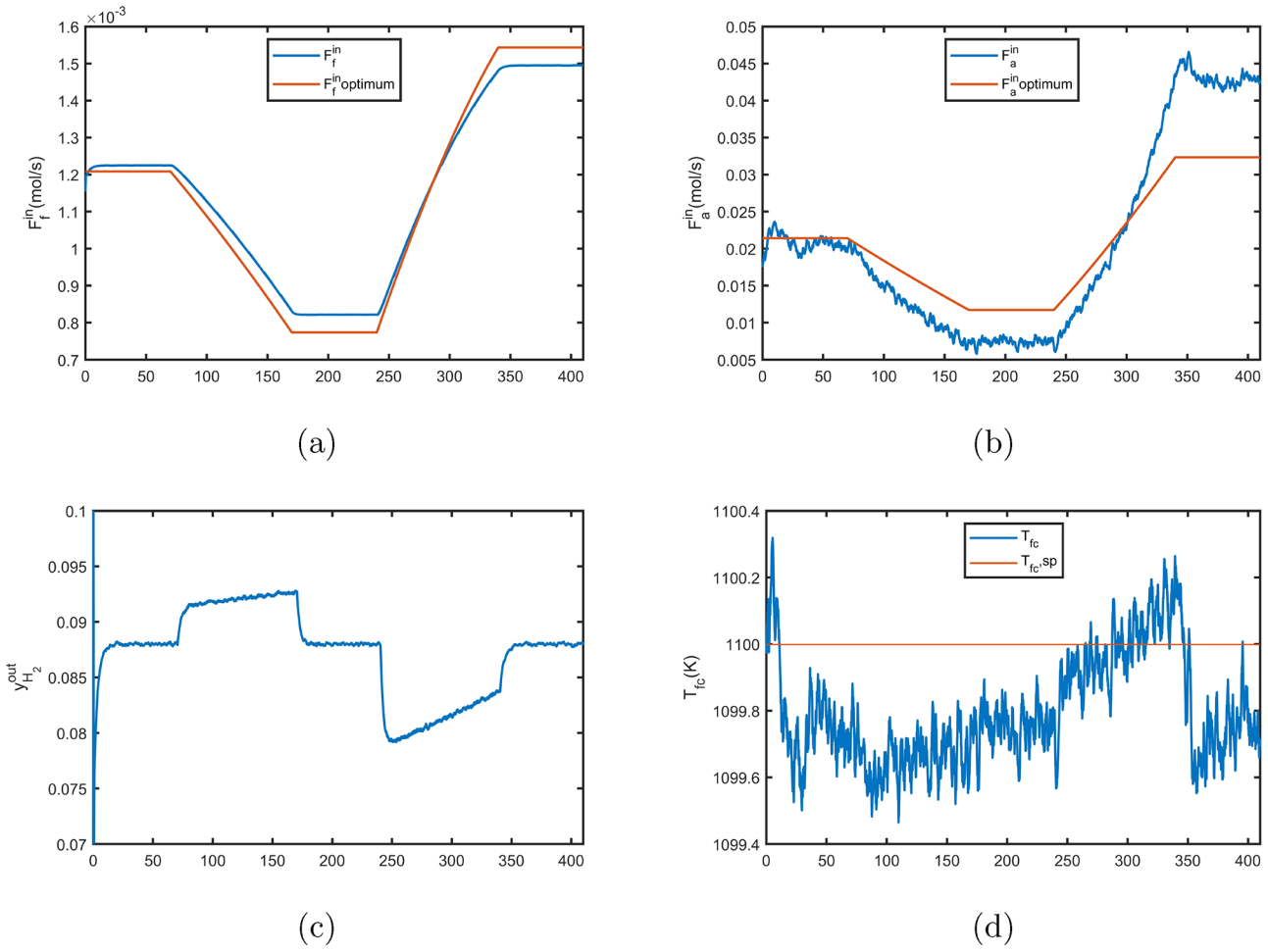

Figure 5. Dynamic simulation of the single layer control structure. (a−d) CVs and MVs in loops 1 and 2, respectively.

Nevertheless, it seems paradoxical that the static calculation with $y_{CH_4}^{out}$ as the CV has many cases of no solution when the current density deviates greatly from the nominal value. It implies that methane is not a good choice for a controlled variable. The proof process is as follows. The material equation in section 2.2 easily proves the following equation.

$$y_{H_2}^{out} = \frac{(R_{(i)}A + y_{CH_4}^{out}\sum C)y_{H_2}^{in} + 3R_{(i)} + R_{(ii)} - R_{(v)}}{2R_{(i)}y_{CH_4}^{in} + R_{(i)}A} \tag{36}$$

where

$$\sum C = \sum_{i=\{CH_4,CO,\ldots,CO_2\}} \sum_{k=\{(i),(ii),(v)\}} R_k V_{i,k} A \tag{37}$$

When the cell temperature T_{fc} is considered an active constraint, $R_{(i)}$ can be approximated as a linear function of $y_{CH_4}^{out}$ and the coefficient is $k_0 \exp\left(\frac{-E_a}{RT_{fc}}\right)$, which is set as C_1. Consequently

$$y_{H_2}^{out} = \frac{2Ay_{H_2}^{in}C_1y_{CH_4}^{out} + (Ay_{H_2}^{in} + 3)C_1y_{CH_4}^{out} + R_{(ii)} - R_{(v)}}{2R_{(i)}y_{CH_4}^{in} + R_{(v)}A} \tag{38}$$

For $y_{H_2}^{out}$ to be greater than 0, $y_{CH_4}^{out}$ needs to meet the following conditions:

$$y_{CH_4}^{out} > \frac{-(Ay_{H_2}^{in} + 3)C_1 + \sqrt{(Ay_{H_2}^{in} + 3)^2C_1^{\,2} - 4[2Ay_{H_2}^{in}C_1(R_{(ii)} - R_{(v)})]}}{4Ay_{H_2}^{in}C_1} \tag{39}$$

$y_{H_2}^{in}$ and $R_{(ii)}$ change very little when $y_{CH_4}^{out}$ is set at different values, but the greater variation in current density will make it impossible to meet the above requirements. In the experiment, this would manifest as the rapid consumption of hydrogen when the current density is too high, causing the surge of concentration overpotential loss. The set-point of $y_{CH_4}^{out}$ needs to allow for a large back-off for changing interference so that the global economic loss will lag behind other measurements. There are almost no control schemes that take the outlet components of carbon dioxide, water, and carbon monoxide as CVs. In addition to the consideration of low controllability, it is also because the calculation shows that these schemes are not suitable for improving the cell efficiency in the global range.

4.2. Selection of Self-Optimizing Controlled Variables. Based on the gSOC method introduced above, the Monte Carlo simulation method is first used to generate 1000

https://doi.org/10.1021/acsomega.3c00293
ACS Omega 2023, 8, 14558−14571

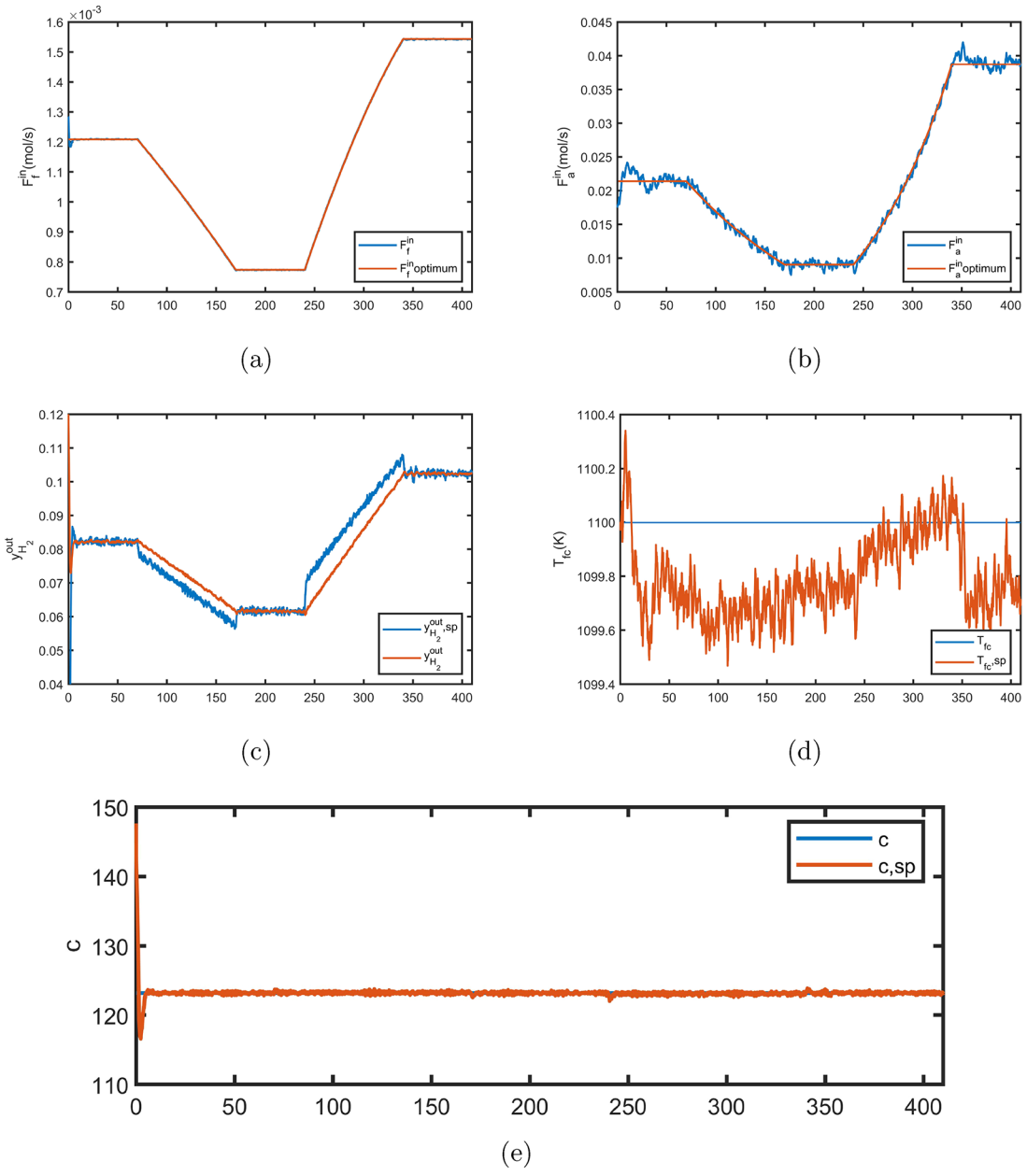

Figure 6. Dynamic simulation of the retrofit SOC scheme. (a−e) CVs and MVs in loops, 1, 2, and 3, respectively.

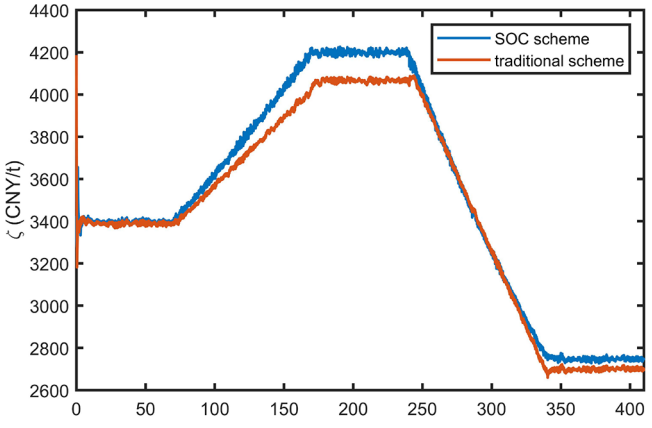

Figure 7. Dynamic trajectories of the economic function.

random disturbance scenario sequences, which is enough to ensure the reliability of calculation of average loss. The SQP method is used to optimize all disturbance scenarios, and the optimal measurements are obtained and stored, where the measurements are

$$y = \{y_{CH_4}^{out}, y_{CO}^{out}, y_{H_2O}^{out}, y_{H_2}^{out}, y_{CO_2}^{out}, y_{O_2}^{out}, F_f^{out}, F_a^{out}, V_{fc}, U_f, \lambda_{air}, F_f^{in}, F_a^{in}\} \quad (40)$$

The measurement noise is considered zero-mean Gaussian noise with a standard deviation of 2% of the nominal value of the process variable. Then, by definition, we construct our matrix W_n and get $\tilde{Y}$ from (34). The finite difference method calculates the sensitivity matrix $G_{y,ref}$ and $J_{uu,ref}$. The numerical solutions of the two matrices are in (41) and (42).

$$J_{uu,ref} = 19421.94 \quad (41)$$

https://doi.org/10.1021/acsomega.3c00293
ACS Omega 2023, 8, 14558−14571

$$G_{y,\mathrm{ref}} = [0 \quad -0.17 \quad -1.84 \quad 7.27 \quad -7.20 \quad 1.94 \quad 0.96 \quad -0.023 \quad 1 \quad -10.1 \quad 11.8 \quad 405.24 \quad -0.015 \quad 1]^{\mathrm{T}} \tag{42}$$

The temperature is determined as an active constraint and consumes one degree of freedom. Here, the inlet air rate is taken as the remaining unconstrained degree of freedom. The derivative of the outlet methane fraction to the control variable is very small, which means that the change of the inlet air rate has little effect on the steam reforming reaction in the case of excess air supply. Outlet fractions of hydrogen and water vapor are most affected by the air inlet rate. The increase of the inlet air rate promotes the hydrogen oxidation reaction and the water gas shift reaction, which results in the decrease of the theoretical open-circuit voltage and the increase of the concentration overpotential loss. Therefore, the derivative of voltage to inlet air rate is negative.

In the analysis of dy/dd, the current density has the greatest influence on the voltage, fuel utilization coefficient, and air ratio. The steam to carbon ratio mainly affects the outlet fractions of water and carbon dioxide. The influence of the pre-reforming degree and inlet temperature on output variables is the least.

The set-points and coefficients of the candidate measurement subsets are calculated according to (35). In the following, the efficiency of the traditional decentralized control structure is evaluated, and the global loss of the measurement combination is exhaustively calculated to determine the appropriate double-layer structure.

In general, the more output variables used to construct CVs, the better the self-optimization performance. However, from a practical point of view, it is encouraged to use fewer output variables, making the form of CVs simple and easy to understand and reducing the measurement cost.[49] Since the lumped parameter SOFC problem is medium-sized, we are allowed to directly use the exhaustive method.

As shown in Table 5, we enumerate all possibilities for subset selection, with the number of measurements selected ranging from 1 to 13. The increase of the subset size gradually decreases the economic loss. When the open-loop control strategy is adopted, i.e., $n_y = 1$, the minimum average loss is 31.77 CNY·t^{-1} and the worst-case loss is 112.70 CNY·t^{-1}, indicating poor economic conditions. When $n_y = 3$, the optimal inclusion measurement is [$y^{\mathrm{out}}_{\mathrm{H_2}}$, $y^{\mathrm{out}}_{\mathrm{CO_2}}$, V_{fc}], with a slight average loss of 0.59 CNY·t^{-1} and the worst-case loss is 4.99 CNY·t^{-1} and therefore acceptable. It is worth mentioning that, when the number of measurements selected is greater than three, the average loss and the worst loss decrease very slowly but the CV becomes increasingly complex. On the basis of these observations, we finally choose to adopt the three-measurement CV, as shown in Table 5. The gSOC method gives the following self-optimized CV and set-point.

$$c_3 = Hy = [326.79 \quad -161.89 \quad 174.38] \begin{bmatrix} y^{\mathrm{out}}_{\mathrm{H_2}} \\ y^{\mathrm{out}}_{\mathrm{CO_2}} \\ V_{\mathrm{fc}} \end{bmatrix} \tag{43}$$

$$\text{set point:} \quad 123.17 \tag{44}$$

Figure 4 shows the maximum efficiency loss caused by different disturbances deviating from the nominal value when control schemes in Table 5 are selected. Obviously, the current density and steam to carbon ratio are the main factors of efficiency loss of the SOFC control system. The gSOC method has an excellent control effect on the two items. Surprisingly, the variations of the inlet temperature and pre-reforming made little difference. Notably, the measurement noise will damage economic efficiency when too many measurements are used to construct CVs.

4.3. Control Reconfiguration. Following the two-layer design method in section 3.3, we constitute a novel control structure for the SOFC. Therefore, this section focuses on comparing the dynamic performances of the traditional decentralized control and the modified two-layer control.

Chatrattanawet et al.[1] reported the control strategy that adjusts the inlet molar flow rate of the fuel and air stream, performing well in controllability analysis. The pairing relationship is $F^{\mathrm{in}}_{\mathrm{f}} \leftrightarrow y^{\mathrm{out}}_{\mathrm{CH_4}}$ and $F^{\mathrm{in}}_{\mathrm{a}} \leftrightarrow T_{\mathrm{fc}}$. However, as mentioned in section 4.1, the methane fraction as the CV is not a reasonable choice while real-time measurement of the hydrogen fraction can reduce concentration overpotential loss and efficiency loss. The cell temperature has been identified as an active constraint and a CV closely related to the inlet air stream. Therefore, the pairing relationships of the lower loop in this paper are $F^{\mathrm{in}}_{\mathrm{f}} \leftrightarrow y^{\mathrm{out}}_{\mathrm{H_2}}$ and $F^{\mathrm{in}}_{\mathrm{a}} \leftrightarrow T_{\mathrm{fc}}$. An additional loop is configured to control the measurement combination c_3 selected by SOC methods by manipulating the set-point of $y^{\mathrm{out}}_{\mathrm{H_2}}$.

We again stress that SOC does not require online identification and repeated optimization calculation of disturbances; therefore, the conventional proportional−integral (PI) controllers here can meet the requirements of device operation. We adjust the bottom loop sequentially and add the top SOC loop, where the simple internal model control (SIMC) rule adjusts the controller parameters. Table 6 shows the reference values of proportional−integral−derivative (PID) parameters. Note that, due to the complex dynamic nature of the SOFC process, there is no guarantee that these parameters will be optimal for the dynamic regulatory control in general. Alternatively, in the following the focus will be placed on the economic performance of the CV when tracked at the set-point.

We have designed many groups of dynamic comparative experiments to verify the effectiveness of the newly designed control structure. Only one of them is shown below.

1. SOFC processes are run under nominal conditions:

d_{nom} = [5000, 2.5, 10%, 1023]

2. In 70 s, interference is changed to random scenario 1.

d_1 = [3000, 2, 8%, 1003]

3. Switch to random scenario 2 at 240 s.

d_2 = [7000, 3, 12%, 1035]

The disturbances will be simulated through a ramping signal lasting 100 s to prevent big oscillations due to large and sudden disturbances, which may be rare in practice. Another consideration is that T_{fc} introduces a slight retreat of 0.25 K to allow dynamic temperature changes moderately.

https://doi.org/10.1021/acsomega.3c00293
ACS Omega 2023, 8, 14558−14571

As shown in Figures 5 and 6, the single-layer control structure is compared with the new two-layer structure configured by the SOC approach. Both methods show excellent temperature control in the presence of operating condition changes. The difference is that the $y_{H_2}^{out}$ was manipulated to remain at about 0.0088 mol/s in the single-layer control while the set-point of $y_{H_2}^{out}$ is now adaptively changed to track the identified self-optimizing variable c_3 for the SOC scheme. Here the set-point for c_3 is 123.12. Due to the SOC layer's guiding effect on the set-point of $y_{H_2}^{out}$, the distance between the control variables and their optimum is far less than that for the single-layer scheme. For the economic performance, the profit function of the SOC scheme is closer to the desired optimal value, as shown in Figure 7. It can be seen that, under nominal conditions (0−70 s), their economic profits are almost identical (nominal optimal). Occasionally, the single-layer control is even better than two-layer control because gSOC seeks the optimal set-point for minimization of the average efficiency, not for the single nominal point. In the d_1 scenario (170−240 s), the single-layer control structure's profit is about 4050 CNY·t^{-1}, while the profit of the SOC scheme approximately increases to 4200 CNY·t^{-1}. In d_2, the profits of the two schemes are 2688 and 2762 CNY·t^{-1}, respectively. Substantial disturbance scenarios have been investigated, and similar results are obtained. These experiments show that the self-optimizing structure is superior to the single-layer structure in terms of the SOFC efficiency.

5. CONCLUSIONS

In this paper, we presented a two-layer self-optimizing control structure for efficiency maximization of a direct internal reforming SOFC. Unlike most previous design methods that focused on power-demand following or system controllability, we aim to improve the fuel efficiency while reducing carbon emission. A reasonable outcome is that the stack temperature T_{fc} is a controlled variable to maintain output performance and restrict the thermal gradient. Besides, the outlet hydrogen fraction $y_{H_2}^{out}$ was evaluated as the optimal CV among substantial process outputs. The lower control layer for the SOFC is configured as $F_f^{in} \leftrightarrow y_{H_2}^{out}$ and $F_a^{in} \leftrightarrow T_{fc}$.

The efficiency performance of the lower control layer is further enhanced by the upper SOC layer, where a combination of measurements

$$c_3 = 326.79y_{H_2}^{out} - 161.89y_{CO_2}^{out} + 174.38V_{fc}$$

(set-point 123.17) is selected as the CV. The two layers are configured in a cascaded architecture, where the set point of $y_{H_2}^{out}$ is adjusted to regulate c_3 at its constant set-point. As shown in section 4, the proposed configuration significantly improved the economic performance of the SOFC. Practically, such a two-layer control structure is convenient for monitoring the underlying variable and saves the maintenance cost because it allows modification on the basis of the existing structure.

In future work, several promising topics can be considered to further improve the efficiency performance for the SOFC power generation process.

1. In the case of frequent operating condition changes, using advanced controllers for CV tracking can improve the transient performances such that the dynamic efficiency is enhanced.

2. A distributed parameter model can constrain the local temperature gradient, which was not investigated in this present work. However, developing a distributed parameter model requires extensive computations, especially in the context of dynamic control of the SOFC. Currently, such a work is under way for the whole SOFC stack.

3. In practice, real measurement of the output variables may have a long time delay and/or errors. Efficient soft sensors for indirect inferences for the gas compositions deserve better developments.

AUTHOR INFORMATION

Corresponding Author

Lingjian Ye − *Huzhou Key Laboratory of Intelligent Sensing and Optimal Control for Industrial Systems, School of Engineering, Huzhou University, Huzhou 313000, China; Key Laboratory of Intelligent Manufacturing Quality Big Data Tracing and Analysis of Zhejiang Province, China Jiliang University, Hangzhou 310018, China;* orcid.org/0000-0001-8732-593X; Email: lingjian.ye@zjhu.edu.cn

Authors

Shengdong Fu − *School of Control Engineering, Zhejiang University, Hangzhou 310027, China; School of Information Science and Engineering, NingboTech University, Ningbo 315100, China*

Feifan Shen − *School of Information Science and Engineering, NingboTech University, Ningbo 315100, China;* orcid.org/0000-0002-7086-6710

Yuchen He − *Key Laboratory of Intelligent Manufacturing Quality Big Data Tracing and Analysis of Zhejiang Province, China Jiliang University, Hangzhou 310018, China;* orcid.org/0000-0002-0528-2778

Complete contact information is available at: https://pubs.acs.org/10.1021/acsomega.3c00293

Notes

The authors declare no competing financial interest.

ACKNOWLEDGMENTS

Financial support from the National Natural Science Foundation of China (61673349), Key Laboratory of Intelligent Manufacturing Quality Big Data Tracing and Analysis of Zhejiang Province, China Jiliang University (ZNZZSZ-CJLU2022-04), and Huzhou Key Laboratory of Intelligent Sensing and Optimal Control for Industrial Systems (2022-17) is acknowledged.

NOMENCLATURE

A	solid oxide fuel cell area (m^2)
c_p	heat capacity (kJ kg^{-1} K^{-1})
D_{eff}	effective diffusivity coefficient (m^2 s^{-1})
E_a	activation energy (kJ mol^{-1})
E_0	open-circuit potential at standard temperature, pressure, and unit activity (V)
$E_{electrode}$	activation energy of electrode exchange current density (kJ mol^{-1})
F	Faraday's constant (C mol^{-1})
F_i	molar flow rate of species i (mol s^{-1})
$(\Delta H)_k$	heat absorption and release of reaction k (kJ mol^{-1})
j	current density (A m^{-2})
$j_{0,electrode}$	exchange current density (A m^{-2})

https://doi.org/10.1021/acsomega.3c00293
ACS Omega 2023, 8, 14558−14571

$k_{electrode}$ pre-exponential factor of electrode exchange current density (A m^{-2})
k_0 pre-exponential constant (mol s^{-1} m^{-2} bar^{-1})
$\dot{m}_i$ mass of component i supplied to system per second (kg s^{-1})
n number of electrons participating in electrochemical reaction
n_i molar concentration of component i (mol m^{-3})
P pressure (bar)
p_i partial pressure of component i in relevant gas channel (bar)
P_{CH_4} price of CH_4 (CNY (kg of CH_4)$^{-1}$)
P_{ele} electricity price (CNY (kWh)$^{-1}$)
P_w power generation of system (kW)
$\dot{Q}_j$ enthalpy flow in flow j (J s^{-1})
R_k rate of reaction k (mol m^{-2} s^{-1})
R gas constant (kJ mol^{-1} K^{-1})
T_{fc} inner temperature (K)
T_{in} inlet temperature (K)
Tax_{CO_2} tax price released by system (CNY (kg of CO_2)$^{-1}$)
V_{fc} potential (V)
E_{OCV} open-circuit potential (V)
U_f fuel utilization factor (%)
$v_{i,k}$ stoichiometric coefficient of component i in reaction k
V_{SOFC} volume of SOFC (m^3)
y_i molar fraction of component i (%)

Greek Symbols

α transfer coefficient
η voltage loss (V)
σ_i electronical conductivity (Ω^{-1} m^{-1})
λ_{air} inverse of air utilization factor
ρ_{SOFC} density (kg m^{-3})
τ_i thickness of layer i (m)

Subscripts

a air channel
act activation
conc concentration
f fuel channel
i component
j flow
k reaction
ohm ohmic
TPB three-phase boundary
PEN PEN structure

Superscripts

in inlet of channel
out outlet of channel

REFERENCES

(1) Chatrattanawet, N.; Skogestad, S.; Arpornwichanop, A. Control structure design and dynamic modeling for a solid oxide fuel cell with direct internal reforming of methane. *Chem. Eng. Res. Des.* **2015**, *98*, 202−211.

(2) Aguiar, P.; Adjiman, C.; Brandon, N. Anode-supported intermediate-temperature direct internal reforming solid oxide fuel cell: Ii. model-based dynamic performance and control. *J. Power Sources* **2005**, *147* (1−2), 136−147.

(3) Shiratori, Y.; Yamakawa, T.; Sakamoto, M.; Yoshida, H.; Kitaoka, T.; Tran, Q. T.; Doan, D. C. T.; Dang, M. C. Biogas production from local biomass feedstock in the mekong delta and its utilization for a direct internal reforming solid oxide fuel cell. *Front. Environ. Sci.* **2017**, *5*, 25.

(4) Escudero, M.; Maffiotte, C.; Serrano, J. Long-term operation of a solid oxide fuel cell with moni−ceo2 as anode directly fed by biogas containing simultaneously sulphur and siloxane. *J. Power Sources* **2021**, *481*, 229048.

(5) Illathukandy, B.; Saadabadi, S. A.; Kuo, P.-C.; Wasajja, H.; Lindeboom, R. E.; Vijay, V.; Aravind, P. Solid oxide fuel cells (sofcs) fed with biogas containing hydrogen chloride traces: Impact on direct internal reforming and electrochemical performance. *Electrochim. Acta* **2022**, *433*, 141198.

(6) Kupecki, J.; Motylinski, K.; Milewski, J. Dynamic analysis of direct internal reforming in a sofc stack with electrolyte-supported cells using a quasi-1d model. *Applied Energy* **2018**, *227*, 198−205.

(7) Recknagle, K. P.; Williford, R. E.; Chick, L. A.; Rector, D. R.; Khaleel, M. A. Three-dimensional thermo-fluid electrochemical modeling of planar sofc stacks. *J. Power Sources* **2003**, *113* (1), 109−114.

(8) Zhang, Z.; Yue, D.; Yang, G.; Chen, J.; Zheng, Y.; Miao, H.; Wang, W.; Yuan, J.; Huang, N. Three-dimensional cfd modeling of transport phenomena in multi-channel anode-supported planar sofcs. *Int. J. Heat Mass Transfer* **2015**, *84*, 942−954.

(9) Wang, Y.; Ren, J.; Shi, Y.; Li, X. Numerical model of direct internal reforming sofc: A comparison between anode-support and metal-support. *ECS Trans.* **2019**, *91* (1), 2013.

(10) Sohn, S.; Baek, S. M.; Nam, J. H.; Kim, C.-J. Two-dimensional micro/macroscale model for intermediate-temperature solid oxide fuel cells considering the direct internal reforming of methane. *Int. J. Hydrogen Energy* **2016**, *41* (12), 5582−5597.

(11) Braun, R. J. *Optimal Design and Operation of Solid Oxide Fuel Cell Systems for Small-Scale Stationary Applications*. Ph.D. Thesis, The University of Wisconsin—Madison, 2002.

(12) Aguiar, P.; Adjiman, C.; Brandon, N. P. Anode-supported intermediate temperature direct internal reforming solid oxide fuel cell. i: model-based steady-state performance. *J. Power Sources* **2004**, *138* (1−2), 120−136.

(13) Kang, Y.-W.; Li, J.; Cao, G.-Y.; Tu, H.-Y.; Li, J.; Yang, J. A reduced 1d dynamic model of a planar direct internal reforming solid oxide fuel cell for system research. *J. Power Sources* **2009**, *188* (1), 170−176.

(14) Xi, H.; Varigonda, S.; Jing, B. Dynamic modeling of a solid oxide fuel cell system for control design. In *Proceedings of the 2010 American Control Conference*; IEEE: 2010; pp 423−428.

(15) Kupecki, J.; Wierzbicki, M.; Jagielski, S.; Kluczowski, R.; Motylinski, K.; Skrzypkiewicz, M. Preliminary long-term experimental characterization of a solid oxide fuel cell operated in dir-sofc mode. *ECS Trans.* **2019**, *91* (1), 471.

(16) Barelli, L.; Bidini, G.; Cinti, G.; Ottaviano, A. Sofc regulation at constant temperature: Experimental test and data regression study. *Energy Conversion and Management* **2016**, *117*, 289−296.

(17) Jienkulsawad, P.; Skogestad, S.; Arpornwichanop, A. Control structure design of a solid oxide fuel cell and a molten carbonate fuel cell integrated system: Top-down analysis. *Energy Conversion and Management* **2017**, *152*, 88−98.

(18) Mojaver, P.; Khalilarya, S.; Chitsaz, A.; Assadi, M. Multi-objective optimization of a power generation system based sofc using taguchi/ahp/topsis triple method. *Sustainable Energy Technologies and Assessments* **2020**, *38*, 100674.

(19) Chatrattanawet, N.; Kheawhom, S.; Chen, Y.-S.; Arpornwichanop, A. Design and implementation of the off-line robust model predictive control for solid oxide fuel cells. *Processes* **2019**, *7* (12), 918.

(20) Skogestad, S. Plantwide control: The search for the self-optimizing control structure. *Journal of process control* **2000**, *10* (5), 487−507.

(21) Ye, L.; Cao, Y.; Yuan, X. Global approximation of self-optimizing controlled variables with average loss minimization. *Ind. Eng. Chem. Res.* **2015**, *54* (48), 12040−12053.

https://doi.org/10.1021/acsomega.3c00293
ACS Omega 2023, 8, 14558−14571

(22) Badur, J.; Lemański, M.; Kowalczyk, T.; Ziółkowski, P.; Kornet, S. Zero-dimensional robust model of an sofc with internal reforming for hybrid energy cycles. *Energy* **2018**, *158*, 128−138.
(23) Klotz, D.; Leonide, A.; Weber, A.; Ivers-Tiffée, E. Electrochemical model for sofc and soec mode predicting performance and efficiency. *International journal of hydrogen energy* **2014**, *39* (35), 20844−20849.
(24) Bessler, W. G.; Gewies, S.; Willich, C.; Schiller, G.; Friedrich, K. A. Spatial distribution of electrochemical performance in a segmented sofc: a combined modeling and experimental study. *Fuel Cells* **2010**, *10* (3), 411−418.
(25) Aydın, Ö.; Nakajima, H.; Kitahara, T. Reliability of the numerical sofc models for estimating the spatial current and temperature variations. *Int. J. Hydrogen Energy* **2016**, *41* (34), 15311−15324.
(26) Yaws, C. L. *The Yaws Handbook of Physical Properties for Hydrocarbons and Chemicals: Physical Properties for More than 54,000 Organic and Inorganic Chemical Compounds, Coverage for C1 to C100 Organics and Ac to Zr Inorganics*; Gulf Professional Publishing: 2015.
(27) Faheem, H. H.; Abbas, S. Z.; Tabish, A. N.; Fan, L.; Maqbool, F. A review on mathematical modelling of direct internal reforming-solid oxide fuel cells. *J. Power Sources* **2022**, *520*, 230857.
(28) Zhao, F.; Virkar, A. V. Dependence of polarization in anode-supported solid oxide fuel cells on various cell parameters. *J. Power Sources* **2005**, *141* (1), 79−95.
(29) Huang, S.; Yang, C.; Chen, H.; Zhou, N.; Tucker, D. Coupling impacts of sofc operating temperature and fuel utilization on system net efficiency in natural gas hybrid sofc/gt system. *Case Studies in Thermal Engineering* **2022**, *31*, 101868.
(30) Zhang, L.; Li, X.; Jiang, J.; Li, S.; Yang, J.; Li, J. Dynamic modeling and analysis of a 5-kw solid oxide fuel cell system from the perspectives of cooperative control of thermal safety and high efficiency. *international journal of hydrogen energy* **2015**, *40* (1), 456−476.
(31) Zhang, X.; Chan, S.; Ho, H. K.; Li, J.; Li, G.; Feng, Z. Nonlinear model predictive control based on the moving horizon state estimation for the solid oxide fuel cell. *Int. J. Hydrogen Energy* **2008**, *33* (9), 2355−2366.
(32) Hajimolana, S. A.; Soroush, M. Dynamics and control of a tubular solid-oxide fuel cell. *Ind. Eng. Chem. Res.* **2009**, *48* (13), 6112−6125.
(33) Chen, J.; Li, J.; Zhou, D.; Zhang, H.; Weng, S. Control strategy design for a sofc-gt hybrid system equipped with anode and cathode recirculation ejectors. *Applied Thermal Engineering* **2018**, *132*, 67−79.
(34) Hori, E. S.; Skogestad, S. Selection of controlled variables: Maximum gain rule and combination of measurements. *Ind. Eng. Chem. Res.* **2008**, *47* (23), 9465−9471.
(35) Kariwala, V.; Cao, Y. Bidirectional branch and bound for controlled variable selection part III: Local average loss minimization. *IEEE Trans. Ind. Inf.* **2010**, *6* (1), 54−61.
(36) Cao, Y.; Kariwala, V. Bidirectional branch and bound for controlled variable selection: Part i. principles and minimum singular value criterion. *Comput. Chem. Eng.* **2008**, *32* (10), 2306−2319.
(37) Kariwala, V.; Ye, L.; Cao, Y. Branch and bound method for regression-based controlled variable selection. *Computers & chemical engineering* **2013**, *54*, 1−7.
(38) Halvorsen, I. J.; Skogestad, S.; Morud, J. C.; Alstad, V. Optimal selection of controlled variables. *Ind. Eng. Chem. Res.* **2003**, *42* (14), 3273−3284.
(39) Alstad, V.; Skogestad, S. Null space method for selecting optimal measurement combinations as controlled variables. *Industrial & engineering chemistry research* **2007**, *46* (3), 846−853.
(40) Kariwala, V.; Cao, Y.; Janardhanan, S. Local self-optimizing control with average loss minimization. *Ind. Eng. Chem. Res.* **2008**, *47* (4), 1150−1158.
(41) Alstad, V.; Skogestad, S.; Hori, E. S. Optimal measurement combinations as controlled variables. *Journal of Process Control* **2009**, *19* (1), 138−148.
(42) Darby, M. L.; Nikolaou, M.; Jones, J.; Nicholson, D. Rto: An overview and assessment of current practice. *Journal of Process control* **2011**, *21* (6), 874−884.
(43) Taghizadeh, M.; Hoseintabar, M.; Faiz, J. Frequency control of isolated wt/pv/sofc/uc network with new control strategy for improving sofc dynamic response. *International Transactions on Electrical Energy Systems* **2015**, *25* (9), 1748−1770.
(44) Sendjaja, A. Y.; Kariwala, V. Decentralized control of solid oxide fuel cells. *IEEE Transactions on Industrial Informatics* **2011**, *7* (2), 163−170.
(45) de Avila Ferreira, T.; Wuillemin, Z.; Marchetti, A.; Salzmann, C.; Van Herle, J.; Bonvin, D. Real-time optimization of an experimental solid-oxide fuel-cell system. *J. Power Sources* **2019**, *429*, 168−179.
(46) Arpino, F.; Dell'Isola, M.; Maugeri, D.; Massarotti, N.; Mauro, A. A new model for the analysis of operating conditions of micro-cogenerative sofc units. *international journal of hydrogen energy* **2013**, *38* (1), 336−344.
(47) Larosa, L.; Traverso, A.; Ferrari, M. L.; Zaccaria, V. Pressurized sofc hybrid systems: control system study and experimental verification. *J. Eng. Gas Turbines Power* **2015**, *137* (3), 031602.
(48) Huang, B.; Qi, Y.; Murshed, M. Solid oxide fuel cell: Perspective of dynamic modeling and control. *Journal of Process Control* **2011**, *21* (10), 1426−1437.
(49) Ye, L.; Guan, H. Self-optimizing control of gold cyanidation leaching process. *Control and Decision* **2017**, *32* (3), 481−486.

https://doi.org/10.1021/acsomega.3c00293
ACS Omega 2023, 8, 14558−14571